JOURNAL OF AIRCRAFT
Vol. 38, No. 2, March–April 2001

Aerodynamic Drag Prediction of Helicopter Fuselage

A. Filippone* and J. A. Michelsen†
Technical University of Denmark, 2800 Lyngby, Denmark

A summary of investigations into predictions of the aerodynamic drag of a modular helicopter fuselage (Eurocopter Dauphin DGV 200) is presented. Drag results are shown for two different configurations, Reynolds numbers up to 6×10^7 (flight conditions), with and without support structure of the wind-tunnel model. Numerical accuracy is investigated for one test case using different computational grids. The results are compared with wind-tunnel measurements and show good agreement with the reference data when the influence of the wind-tunnel strut is taken into account. The computational fluid dynamics model developed consists of a parallel multiblock, multigrid Reynolds-averaged Navier–Stokes code and a three-dimensional hyperbolic grid generator. Block-structured grids are generated from a CAD base. From a numerical point of view, convergence was achieved quickly in all of the cases computed, thus showing efficiency and low CPU cost.

Introduction

RECENT progress in computational fluid dynamics (CFD) has stimulated research into numerical prediction of the aerodynamic drag for a variety of aerodynamic components and, more recently, for full aircraft configurations. Navier–Stokes codes are now routinely used for a variety of tasks. The task of predicting the drag is one of the most daunting because the international standards[1] are very demanding and because numerical errors can be of the same order as the drag coefficient. On the other hand, the cost of wind-tunnel facilities often does not allow measurements on a full-scale model and extrapolation of data to flight conditions is known to be cumbersome. A review of the state-of-the-art CFD methods in aeronautics has recently been published by van Dam.[2]

Wind-tunnel measurements are expensive and less flexible than CFD methods. Therefore, there is strong interest in the aircraft industry to develop, validate, and advance computational methods to the point where they can become a valuable aid to the design of an aircraft.

This is particularly important in the case of the helicopter. The drag levels C_D of a typical helicopter are at least 50 times higher than the C_D of a commercial jet aircraft. A good drag coefficient for a clean configuration is $C_D \sim 1$. The Eurocopter AS 365N, whose fuselage is based on the Dauphin model discussed in this paper, after reengineering[3] had a $C_D \sim 1.05$ (down from 1.43). The drag of a helicopter in forward flight is a combination of fuselage resistance, rotor drag, and a complex interference between the components. It is estimated that the fuselage is the cause of up to 50% of the total drag. Drag reduction is a key item in the industry, hence the interest in this particular aspect of aerodynamics.

This paper describes the results obtained within the framework of a much larger European project (Helifuse), whose objectives were twofold: 1) production of an experimental database on modular fuselage geometries (with and without rotor) at flight Reynolds numbers and 2) development and validation of Navier–Stokes methods for the prediction of aerodynamic loads and moments.

The wind-tunnel test program and the results of the experimental tasks of the project have been published by Gatard et al.[4] Development of the Navier–Stokes methods and the comparison among computational activities are discussed by Costes et al.[5]

This study is concerned with the development of a multiblock, multigrid Navier–Stokes code (EllipSys3D) for the calculation of relatively complex aerodynamic flows. Tests have been conducted on two modular fuselage geometries (Fig. 1) at Reynolds numbers ranging from ordinary wind-tunnel tests to full-scale level flight. Models have been created to simulate the effects the discretization errors due to different grids and of the support structure in the wind tunnel.

Received 25 March 2000; revision received 21 November 2000; accepted for publication 30 November 2000.

*Senior Scientist, Institute of Energy Engineering. Member AIAA.
†Senior Scientist, Institute of Energy Engineering.

Fluid Dynamic Model

EllipSys3D[6–8] is a finite volume discretization of the incompressible Reynolds-averaged Navier–Stokes (RANS) equations in general curvilinear coordinates. The RANS equations are written in general curvilinear coordinates The turbulent stresses are modeled by a turbulent eddy viscosity, given by the k–ω baseline model, proposed by Menter.[9]

EllipSys3D uses a collocated variable arrangement, and Rhie and Chow[10] interpolation is employed to avoid odd/even pressure decoupling. As the code solves the incompressible flow equations, no equation of state exists for the pressure, and the SIMPLE procedure of Patankar and Spalding[11] is used to enforce the pressure/velocity coupling. EllipSys3D is parallelized with a message passing interface (MPI) for execution on distributed memory machines using a nonoverlapping domain decomposition technique.

The solution is advanced using local time stepping. In each time step, the momentum equations act as a predictor to advance the solution in time. At this point in the computation the flowfield does not fulfill the continuity equation. The rewritten continuity equation (the pressure correction equation) is used as a corrector enforcing the continuity constraint onto the flowfield. To accelerate the overall algorithm, a three-level grid sequence is used.

The convective terms are discretized by a second-order upwind scheme, using the deferred correction approach first suggested by Khosla and Rubin.[12] Centered differences are used for the diffusive terms.

Computational Mesh

The surface geometry of the helicopter fuselage is defined in an IGES CAD model. The surface mesh, which is needed as basis for the hyperbolic procedure, is of an algebraic type generated by the ICEM/CFD mesh generator. This interface is needed because initial graphics exchange specification (IGES) files are the stardard communication models that describe accurately the CAD object that is passed to the manfacturing department as well as to the CFD engineers. From this description of the object, we can generate surface grids that are sufficiently close to the original model. Figure 2 shows the surface mesh on configuration C2 (see Table 1 for description). The volume mesh is generated by a hyperbolic mesh-generation procedure.

The governing equations for hyperbolic mesh generation are derived from orthogonality relations and a volume constraint,

$$x_\xi x_\zeta + y_\xi y_\zeta + z_\xi z_\zeta = 0 \tag{1}$$

$$x_\eta x_\zeta + y_\eta y_\zeta + z_\eta z_\zeta = 0 \tag{2}$$

and a volume constraint

$$x_\xi y_\eta z_\zeta - x_\xi y_\zeta z_\eta + x_\eta y_\zeta z_\xi - x_\eta y_\xi z_\zeta + x_\zeta y_\xi z_\eta - x_\zeta y_\eta z_\xi = \Delta V \tag{3}$$

The Cartesian coordinates are designated by x, y, and z, and ξ, η, and ζ refer to the transformed coordinates. Marching takes place in the ζ direction, with $\zeta = 0$ denoting the body surface. Here the distribution of $\xi = \text{const}$ and $\eta = \text{const}$, that is, the surface mesh, is user specified. The preceding mesh-generation system is hyperbolic by nature. Oscillations and overlapping of mesh lines may result from discontinuity and, to some extent, from surface curvature. The inclusion of artificial dissipation into the discretized governing equations, as proposed by Steger et al.[13] and Steger and Rizk[14] alleviates problems of this type. Tai and Yin[15] proposed the use of upwind differencing of the governing equations. Inherently adaptive dissipation was obtained, greatly facilitating mesh control. Tai et al.[16] extended the procedure to three dimensions. In the far-field portions of the mesh, where the mesh cells are very tall, the upwind dissipation is not always appropriate, especially not near mesh irregularities. To obtain grid smoothness in the sense adopted by Winslow[17] and Brackbill and Saltzman,[18] a Laplacian term is included in the generation system. For the configuration with strut, an extension of the hyperbolic concept is needed to control the mesh distribution normal to the strut surface. After completion of the hyperbolic mesh generation, the blocks around the strut are remeshed by interpolation along the computed normal mesh lines. The number of cells in the direction normal to the strut is increased to allow appropriate resolution of the boundary layers around the strut.

The grid generation is relatively fast. Once the surface mesh is available in the required format (bottleneck of the process), the program generates grids at the rate of about 1×10^6 cells per minute. These grids can be viewed with any flow visualization program, and corrections can be performed quickly by changing the input data. The visualization phase is essential because of the difficulties of generating diagnostics detailed enough to eliminate all of the typical difficulties relative to complex three-dimensional grids (negative cells, skewness, net density at adjoining block faces/edges, etc.).

Test Matrix

The experiments have been performed in the pressurized wind tunnel ONERA F1 at Le Fauga-Mauzac (France) on a one-quarter scale model of the DGV 200 fuselage Dauphin (Eurocopter). Three

Table 1 Test matrix

Case	Configuration	α, deg	β	Re	M
TC1	C1	0.0016	0.0	6×10^6	0.088
TC2	C1	0.0160	0.0	30×10^6	0.235
TC3	C1	−0.0050	0.0	60×10^6	0.235
TC4	C2	0.0183	0.0	30×10^6	0.235
TC5	C2	−5.1930	0.0	30×10^6	0.235

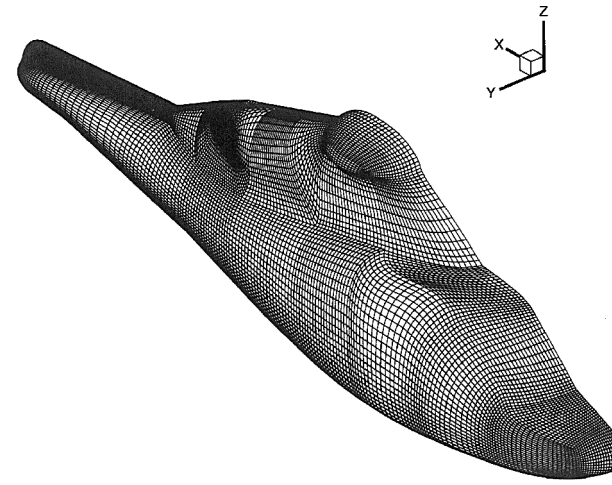

Fig. 2 Surface grid on configuration C2.

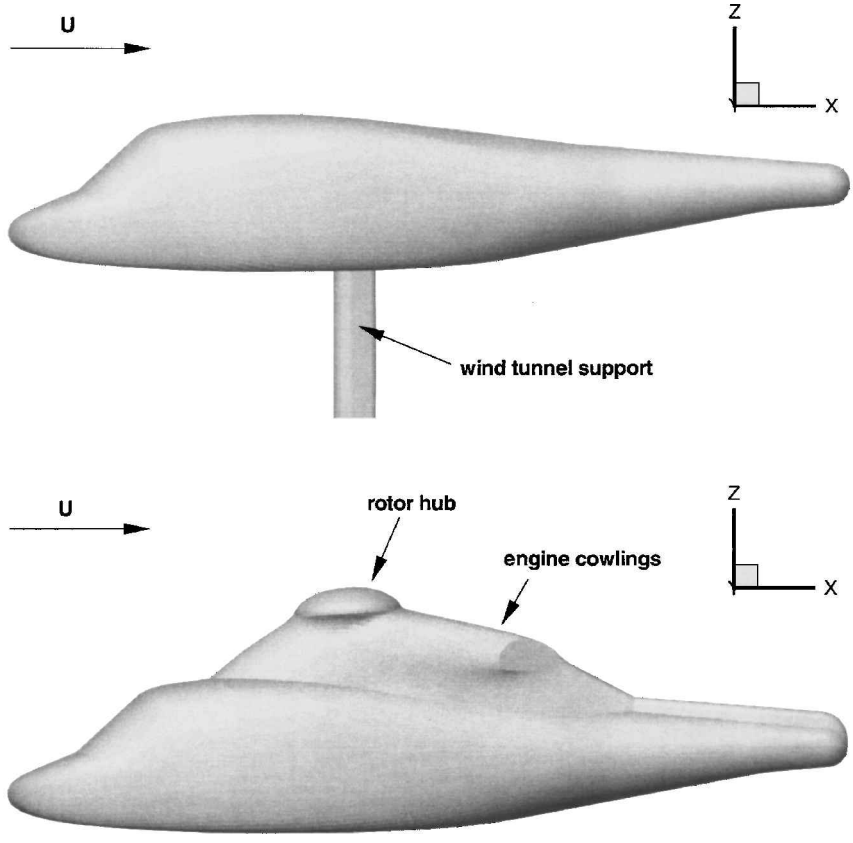

Fig. 1 Configurations C1 (with strut) and C2.

configurations have been considered: the basic fuselage (C1), the fuselage with engine fairings and rotor hub (C2), and the fuselage as C2 plus a five-bladed rotor (C3). The model was supported by a vertical strut positioned at about 39% of the fuselage length from the nose. Configurations C1 and C2 are shown in Fig. 1.

Reynolds numbers ranged between 6 and 6×10^7 (the length scale being the fuselage model), at Mach numbers between 0.088 and 0.235 (pressure in the test section between 1 and 3.85 bars, respectively). The lowest Reynolds number is the Reynolds number considered by industry in ordinary wind-tunnel testing. The highest Reynolds number is a realistic full-scale approximation.

About 200 pressure taps were located on the model (actual number dependent on the configuration). Loads and moments were measured with a six-component balance.

The complete test matrix included angles of attack $\alpha = \pm 5$ deg and yaw angles $\beta = \pm 5$ deg, for a grand total of 72 different operation points, plus a number of conditions for hot-film measurements and acenaphtene visualization (for free turbulent transition analysis) and oil flow visualizations.[4] The analysis of the wind-tunnel data was concerned with test repeatability, strut interference, and deviation of test conditions. It was found that the maximum error is of the order 15% at the lowest Reynolds number and 1.5% at the largest. Influence of the strut on the drag coefficients was difficult to evaluate, but information gathered from industry experts led to the conclusion that it is of the order of three drag counts. The dispersion of the data was estimated from a sample of 30 runs at each operation point. The error on both Reynolds and Mach number was estimated at 0.05%. Repeatability of results was tested by running some operation points twice: All of the results are within the interval of confidence $[-3\sigma, +3\sigma]$, where σ is the standard deviation of the sample.

The test matrix used in the present work is a subset of the wind-tunnel tests and is summarized in Table 1.

Results and Discussion

Configuration C1 (TC1, TC2, TC3) was computed at all of the Reynolds numbers with and without the strut. At the time of the computational task of the project, the actual geometry of the strut was not known. Therefore, it was decided to approximate the support with an arbitrary cross section derived from the analysis of the photographs taken during the experimental phase of the project. Figure 3 shows a detail of the surface grid around the strut with the multiblock structure. This grid is a topological modification of the basic C1 grid, wherein only the blocks affected by the presence of the strut have been redesigned. The height of the wall cell on the strut is about five times larger than the corresponding cell away from the fuselage. This was found to be sufficient to limit the growth of the y^+ values at the junction, where turbulent flow separation occurs.

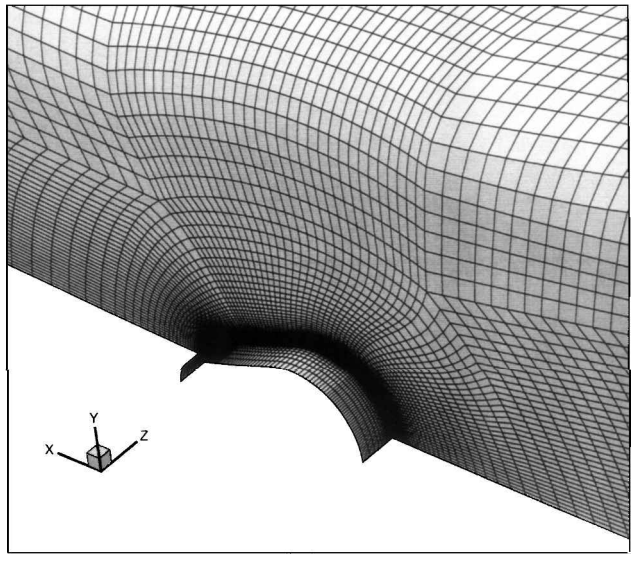

Fig. 3 Grid details with multiblock structure, configuration C1 with strut.

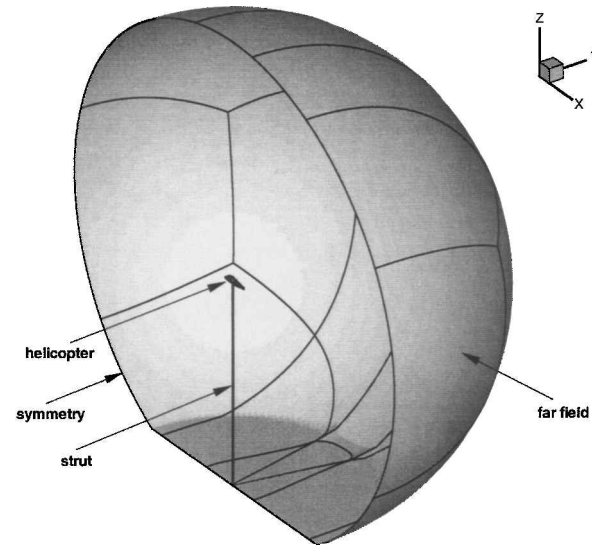

Fig. 4 Computational domain, configuration C1 with strut.

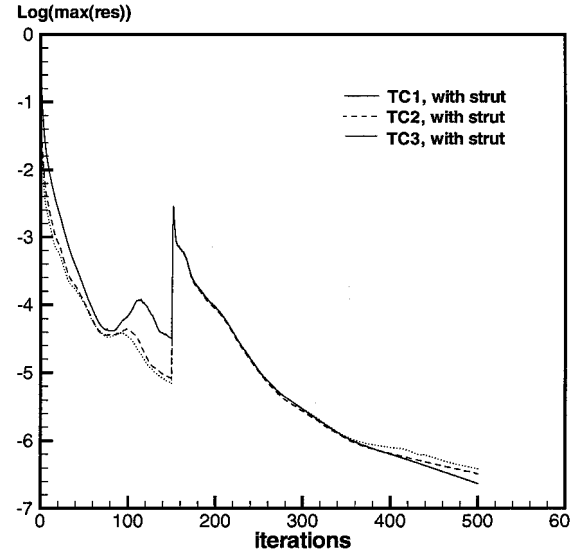

Fig. 5 Iteration history: maximum residual for C1, configuration with strut.

Another important difference is the boundary condition at the confluence between the far field and strut (bottom end of the computational domain shown in Fig. 4). On the symmetry plane, a far-field point meets a wall point at the intersection with the strut. By flattening the bottom by a specified amount and giving the condition of symmetry, this inconsistency is eliminated.

The number of blocks varied from 28 (TC1-TC3, clean) to 99 (TC4, TC5), and the number of cells from 0.918×10^6 (TC1-TC3, clean configuration) to about 1.442×10^6 (TC1-TC3, with the strut). Each block had a cubic structure, $n \times n \times n$ cells.

The parallel version of the code was run on 11 processors of an IBM SP2 computer. The runs required less than 1 h to complete 500 iterations, after which the residual was reduced by six orders of magnitude on the configuration C1 with the strut, as shown in Fig. 5. Configuration C1 without the strut converged a few orders of magnitude higher.

The aerodynamic forces and moments are computed by direct integration of the surface pressure and local skin friction with our own postprocessor. The strut was excluded from the integration of the aerodynamic drag. The C_D values have been rescaled (actual data are proprietary).

Table 2 Test matrix for grid refinement studies, TC2

h_0	y^+	No. of cells
	Test 1	
1.2×10^{-6}	0.81	387,082
1.2×10^{-6}	0.87	746,368
1.2×10^{-6}	0.83	917,504
	Test 2	
1.2×10^{-6}	0.81	917,504
2.4×10^{-6}	1.72	917,504
4.8×10^{-6}	3.41	917,504

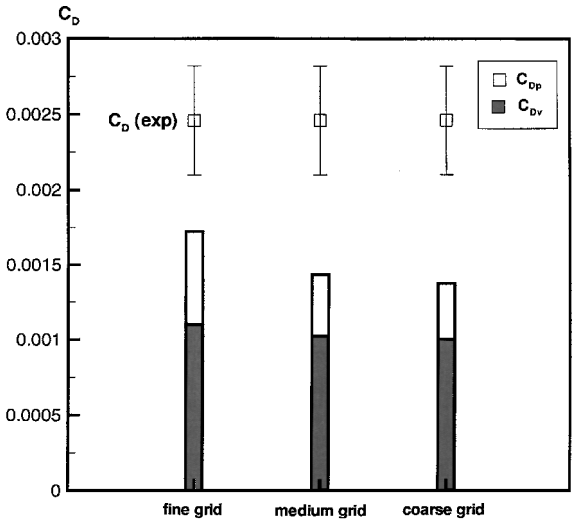

Fig. 6 Grid refinements on TC2: effects of grid size.

Grid Effects

We have performed studies of grid refinements to investigate the effects of numerical dissipation for TC2. The study consisted of 1) grid refinement at constant wall cell height h_0 and 2) decreasing wall cell height. (A third test comparing the performances at different multigrid levels was inconclusive because of too few cells at the coarse levels.)

In the first case we have maintained a constant y^+, while changing the bunching parameter in the hyperbolic grid generation. (The bunching parameter is a parameter affecting the distribution of points along a grid line, and its effects are particularly important within the viscous layers.) In the second case, we have doubled and quadrupled the cell size at the wall while maintaining a constant mesh size. In the last case we have solved the Navier–Stokes equations on three multigrid levels from the finest mesh and compared the results. Table 2 summarizes the runs.

In Table 2, y^+ denotes the maximum value of the nondimensional length scale in the turbulent viscous layer (computed) and h_0 the actual value of the cell height (assigned). Figure 6 shows the results obtained with different grid sizes (test 1). The computed C_D comes closer to the reference data as the grid is refined, with the final refinement more effective than the first. However, it is still below the error band. The results relative to the second test have shown similar tendencies (Fig. 7).

Strut Influence

The addition of the strut to the computational model was expected to improve the predictions at all Reynolds numbers. This was actually the case, as shown in Fig. 8, where it is evidenced that the strut added a contribution of the same order at all Reynolds numbers. The C_D decreases with the increasing Reynolds number, although it is little affected by the speed at $Re > 3 \times 10^7$.

The computed test case TC1 is the closest to the wind-tunnel data when reference is taken with respect to the error band, but it would be the most inaccurate result if the error band were of the same order as the other test cases. Some flow unsteadiness at the base of the strut could account for the wide error band at the lowest Reynolds number. From a computational point of view, the accuracy of the strut geometry could account for at least some pressure component and some skin-friction component in the largely separated wake. Important grid effects have been excluded because the convergence was rapid and the y^+ values at the junction were of the same order of magnitude in both directions.

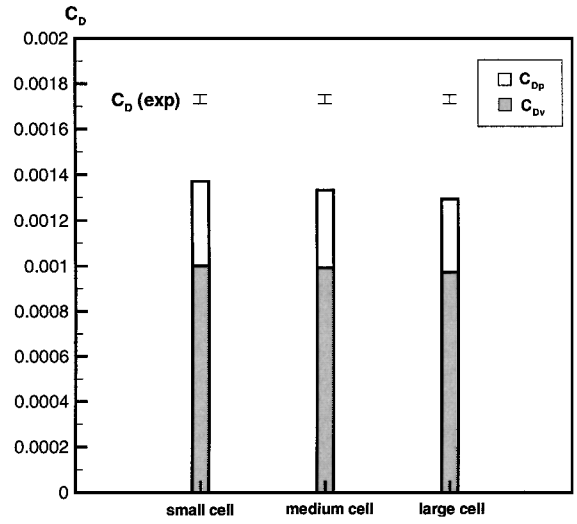

Fig. 7 Grid refinements on TC2: effects of wall cell size.

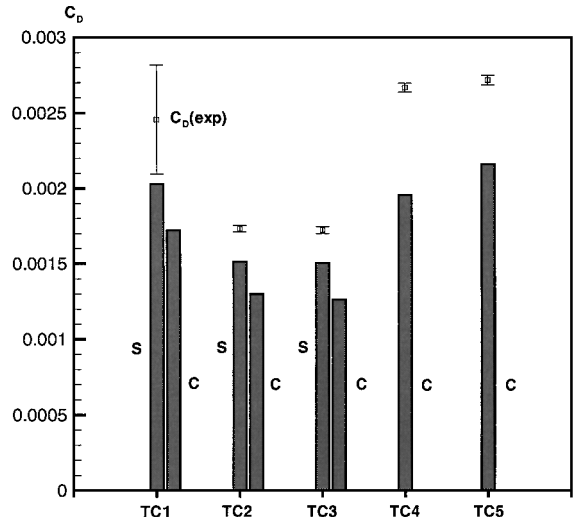

Fig. 8 Computed drag coefficient for all test cases; configuration C1 (test cases TC1, TC2, TC3) shows the results with/without strut: *C* = clean model and *S* = model with strut.

The C_D of configuration C2 is considerably larger than that of the basic geometry because of an extended wetted area and additional flow separation occurring at the base of the engine cowlings and rotor hub. The gap is larger than that evidenced in the basic configuration C1. Although the strut could not be applied to the computational model of C2, it is believed that its effects would be of the same order as they were on configuration C1 because the underbody flow is the most affected by the interference.

Figure 9 shows the drag decomposition (pressure and viscous components). The contribution of the pressure term C_{D_p} increases with the speed and represents about three-quarters of the total drag at the largest Reynolds number. At any given Reynolds number, the pressure component is larger in the configuration with the strut.

The surface pressure distribution at the symmetry lines and at two cross sections upstream and downstream the strut are shown in Figs. 10 and 11 for TC1 and TC3, respectively. Correlation with the

pressure taps is generally good. The most evident effect of the strut appears to be at the bottom symmetry line, in a region of stagnation flow behind the strut's trailing edge.

Configuration C2

The surface grid on this configuration is shown in Fig. 2. The computed drag coefficient for TC4 and TC5 (incidence $\alpha = -5$) is shown in Fig. 8. Although the C_D has increased due to a larger wetted area as well as wider separation regions, it remains below the reference data. Addition of the strut influence is estimated to add a quantity close to that of configuration C1, which would not be enough to close the gap.

The surface pressure distribution for TC5 is shown at the symmetry lines (Fig. 12) and at four cross sections (Fig. 13). The results are generally satisfactory.

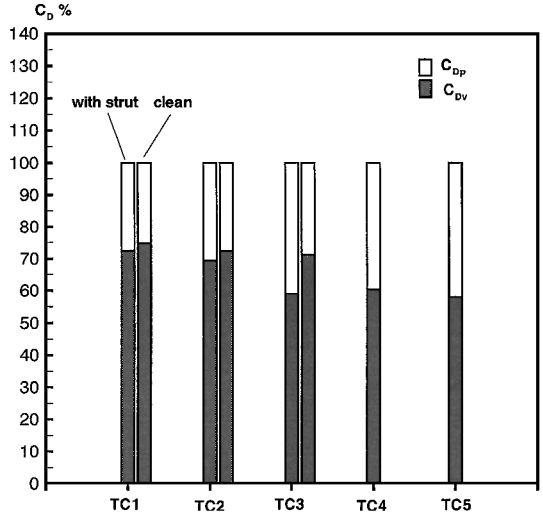

Fig. 9 Drag decomposition for all test cases.

Flow Visualizations

The skin-friction lines give indications of the flow physics, particularly in regions of flow separation and reattachment. This is particularly interesting for the configuration C1 with the strut. The interference effect at the junction is shown in Fig. 14, which is a bottom view of the wind-tunnel model TC1. There is an extended area of separation behind the strut, roughly symmetrical. Flow reattachment appears to occur slightly later. A vortex structure with a focus point is clearly evident.

Figure 15 is a top view of TC4 (configuration C2), with the engine cowlings and the rotor hub. We see a breakdown in the flow symmetry, which was not the case with the CFD model. The agreement of the limiting streamlines around the reattachment line seems satisfactory.

Possible Causes of Inaccuracy

All of the numerical drag predictions are below the wind-tunnel data and outside the error bands. None of the causes of inaccuracy studied could account for the gap in the computed C_D. We have excluded errors in the integration scheme of the postprocessor and due to an insufficient number of grid cells. The geometry model was also under consideration. Inaccuracies could be due to the CAD model, to the surface quality (the CAD model was smoothed to

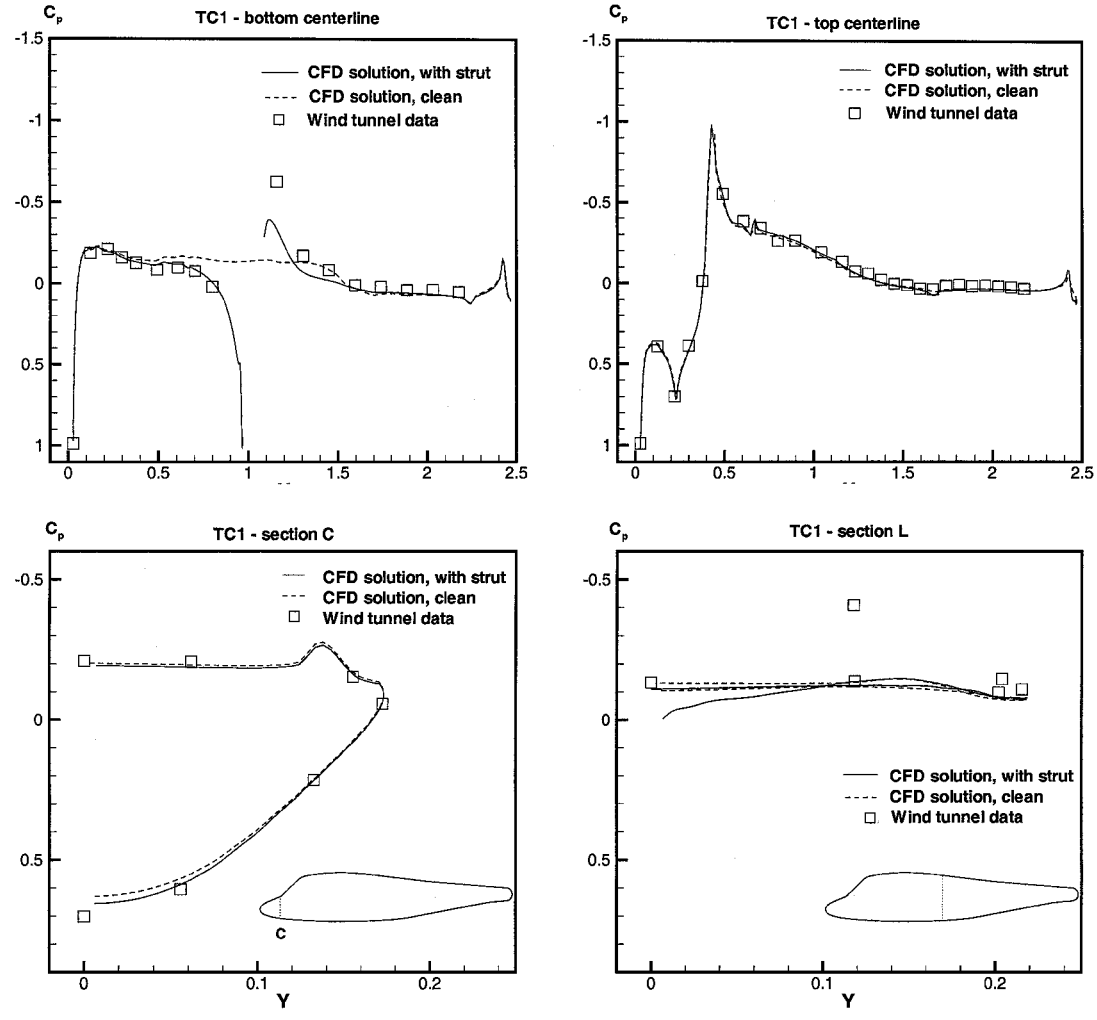

Fig. 10 C_p at symmetry line and cross sections *C* and *L*, test case TC1.

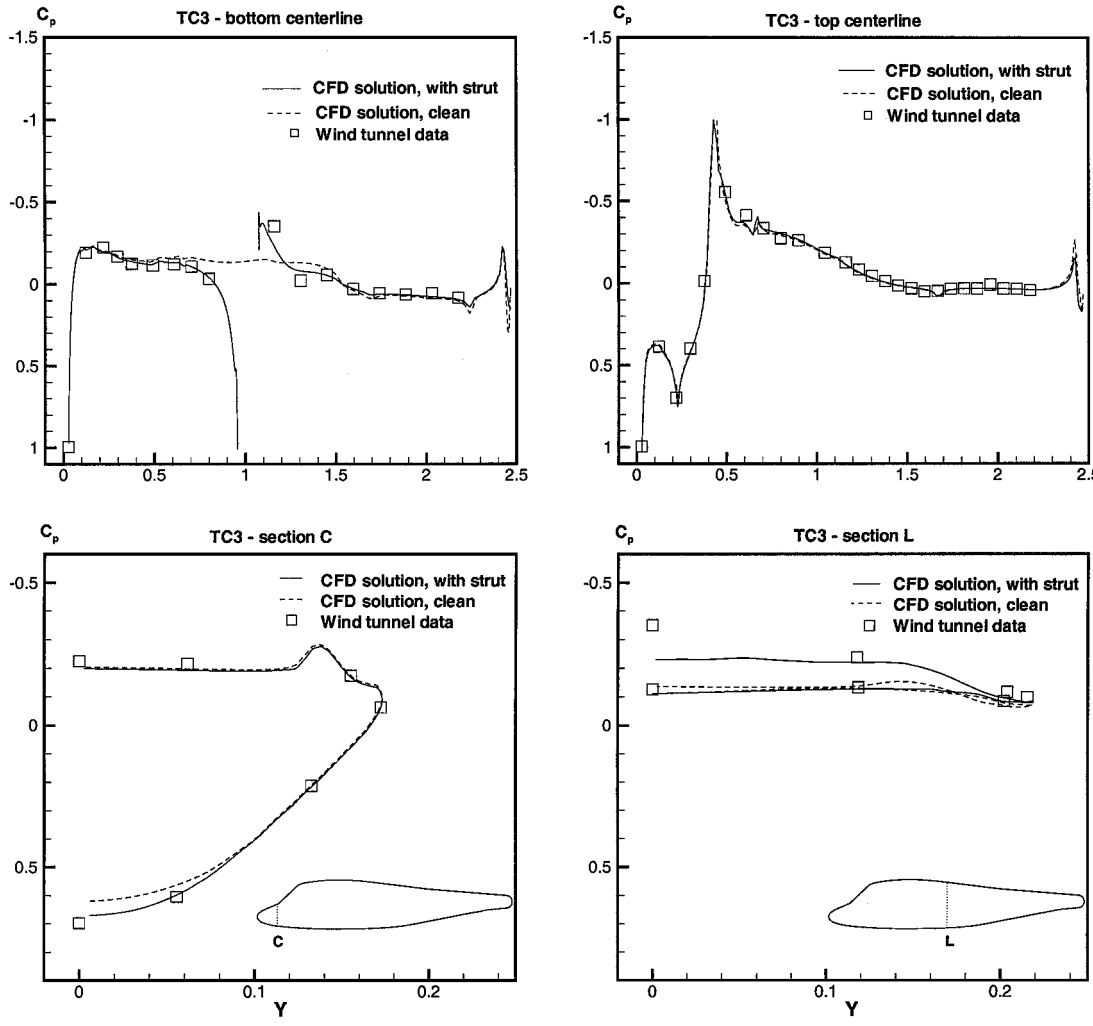

Fig. 11 C_p **at symmetry line and cross sections** C **and** L**, test case TC3.**

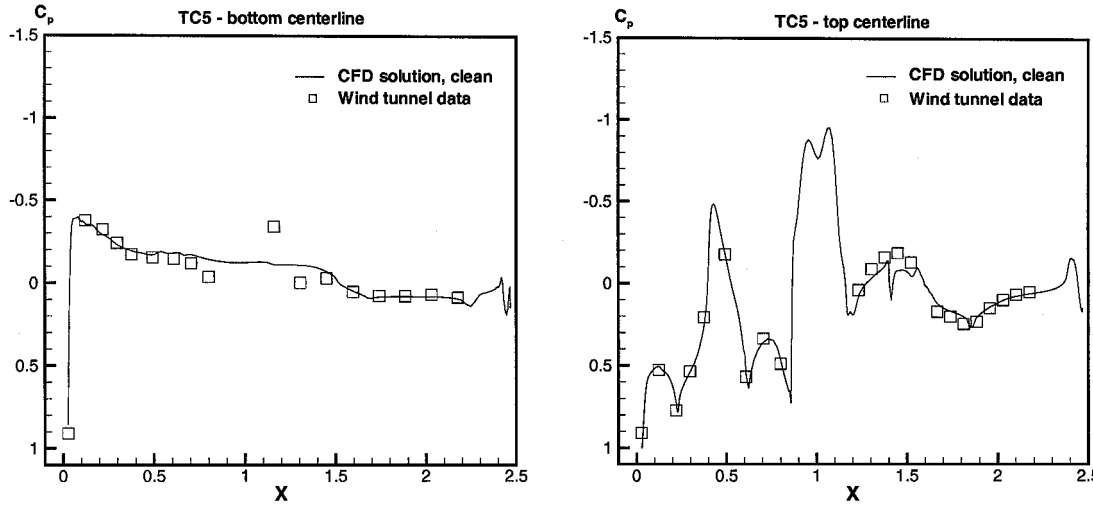

Fig. 12 C_p **at symmetry lines, test case TC5.**

create the CFD grid, although some bumps remained, as shown in cross section C, Figs. 10, 11, and 13), to the actual geometry of the strut (which was different from the wind-tunnel model), to sideslip setting, and to wind-tunnel model symmetry.

As for the wind-tunnel experiments, the accuracy was within three drag counts, and repeatibility of the tests was good. Only TC1 showed a relatively large error bar.

The latter case is worth discussing. Flow visualizations of some test cases (particularly TC4) showed vortices building up unsymmetrically at the fuselage tail, at the base of the rotor hub, and on the engine cowlings. This asymmetry has been suppressed in our computational model because of limitations in the computer power at the time we performed the work, but it could be a cause of inaccuracy on all test cases run with configuration C2.

The turbulence model could not be investigated during the course of this research. Analysis of the skin-friction lines shows some differences in the neighborhood of the separation points, particularly in the cases with the strut (Fig. 14).

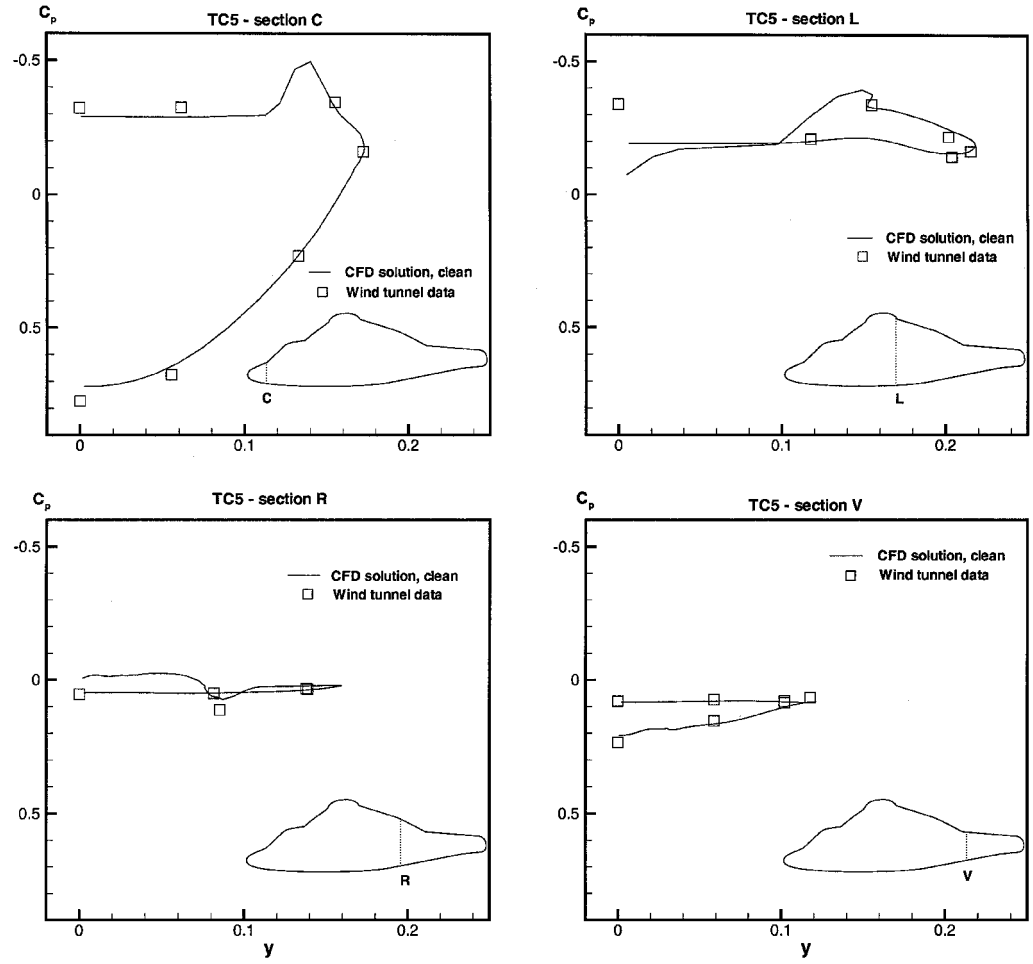

Fig. 13 C_p at sections C, L, R, and V, test case TC5.

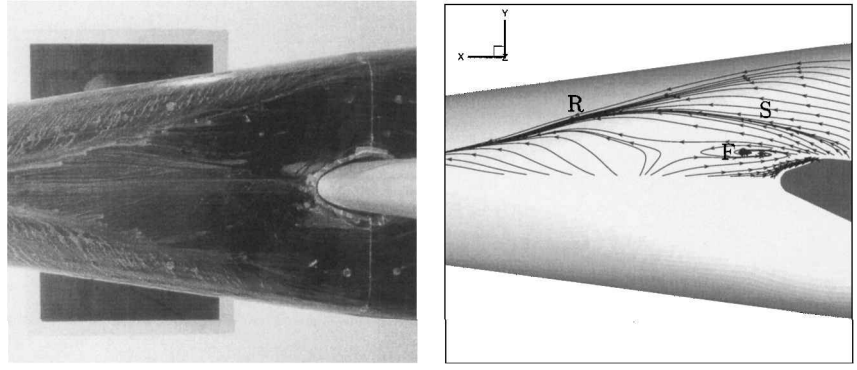

Fig. 14 Flow visualization for TC1, bottom view with the strut: wind-tunnel model at left, CFD model at right (S = separation, R = reattachement, and F = focus).

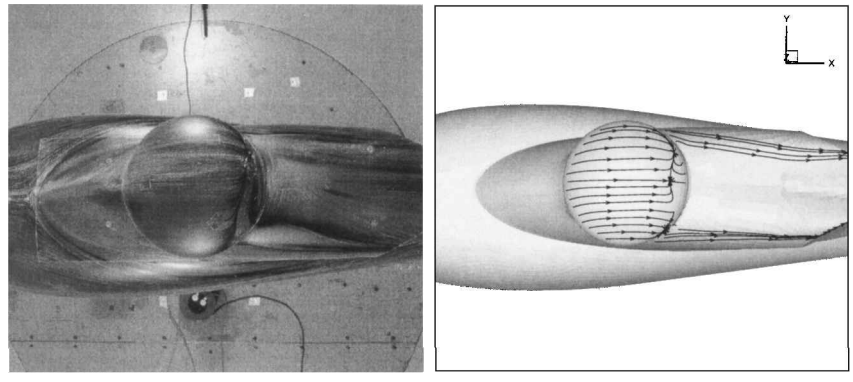

Fig. 15 Flow visualization for TC4, top view of engine cowlings: wind-tunnel model at left, CFD model at right.

Concluding Remarks

This study has shown the present capabilities of a structured Navier–Stokes solver at high Reynolds number. A number of test cases has been selected from a database of wind-tunnel experiments in an attempt to predict the aerodynamic drag of modular shapes of helicopter fuselages. A fast three-dimensional hyperbolic grid generator has been developed for this purpose, and it is now possible to generate grids on relatively complex configurations with moderate concavities. The results presented show that the aerodynamic drag is underpredicted, although the trends are correct in terms of Reynolds number and configuration dependence. A number of investigations into a variety of parameters that could influence the accuracy of the results have been presented, and a number of others have been left open for future study. The constraint of symmetrical flow may not be appropriate for the simulation of more realistic flows with separation. The validation phase presented will prove very useful toward simulating asymmetric flows (with and without yaw) and more complex configurations. The database produced during the experimental phase of the Helifuse project can be used for further code validation. The turn-around time for a given configuration (geometry modeling, grid generation, setting of input files, preprocessing, computation, postprocessing, and presentation of data) has been reduced to a few days. The bottleneck is the grid-generation phase because it requires interface with a CAD system, and the multiblock structure may include too many constraints in the problem.

Acknowledgment

The authors wish to thank the partners of the Helifuse consortium for allowing the publication of the experimental data.

References

[1]"AGARD Wind Tunnel Flow Quality and Data Accuracy Requirements," AR-184, AGARD 1982.

[2]van Dam, C. P., "Recent Experience with Different Methods of Drag Prediction," *Progress in Aerospace Sciences*, Vol. 35, No. 8, 1999, pp. 751–798.

[3]Poisson-Quinton, P., "Parasitic and Interference Drag Prediction and Reduction," *Aircraft Drag Prediction and Reduction*, R-723, AGARD, 1985, pp. 6-1, 6-27.

[4]Gatard, J., Costes, M., Kroll, N., Freiherr von Geyr, H., Renzoni, P., Kokkalis, A., Rocchetto, A., Serr, C., Filippone, A., and Wehr, D., "Helifuse: High-Reynolds Helicopter Fuselage Drag Tests in the ONERA F1 Pressurized Wind Tunnel," *23rd European Rotorcraft Forum*, Dresolen, Germany, Sept. 1997.

[5]Costes, M., Freiherr von Geyr, H., Collercandy, R., Kroll, N., Renzoni, P., Amato, M., Kokkalis, A., Rocchetto, A., Serr, C., Larrey, E., Filippone, A., and Wehr, D., "Computation of Helicopter Fuselage Aerodynamics Using Navier–Stokes CFD Methods," *Journal of the American Helicopter Society*, Vol. 45, Part 3, 2000, pp. 147–156.

[6]Michelsen, J. A., "Basis3D—A Platform for Development of Multiblock PDE Solvers," TR AFM 92-05, Inst. of Energy Engineering, Technical Univ. of Denmark, Lyngby, Denmark, 1992.

[7]Michelsen, J. A., "Block Structured Multigrid Solution of 2D and 3D Elliptic PDE's," TR AFM 94-06, Inst. of Energy Engineering, Technical Univ. of Denmark, Lyngby, Denmark, 1994.

[8]Sørensen, N. S., "General Purpose Flow Solver Applied to Flow over Hills," Ph.D. Dissertation, Rept. Risø-R-827(EN), Wind Energy Dept. Risø National Lab., Roskiede, Denmark, 1995.

[9]Menter, F. R., "Zonal Two Equation k–ω Turbulence Models for Aerodynamic Flows," AIAA Paper 93-2906, Aug. 1993.

[10]Rhie, C. M., and Chow, W. L., "A Numerical Study of the Flow Past an Isolated Airfoil with Separation," *AIAA Journal*, Vol. 21, No. 10, 1983, pp. 1525–1532.

[11]Patankar, S. V., and Spalding, D. B., "A Calculation Procedure for Heat, Mass, and Momentum Transfer in Three Dimensional Parabolic Flows," *International Journal of Heat and Mass Transfer*, Vol. 15, 1972, pp. 1787–1806.

[12]Khosla, P. K., and Rubin, S. G., "A Diagonally Dominant Second-Order Accurate Implicit Scheme," *Computers and Fluids*, Vol. 2, No. 2, 1974, pp. 207–209.

[13]Steger, J. L., and Chaussee, D. S., "Generation of Body-Fitted Coordinates Using Hyperbolic Partial Differential Equations," *SIAM Journal on Scientific and Statistical Computing*, Vol. 1, No. 4, 1980, pp. 431–437.

[14]Steger, J. L., and Rizk, Y. M., "Generation of Three-Dimensional Body-Fitted Coordinates Using Hyperbolic Partial Differential Equations," NASA TM 86753, 1985.

[15]Tai, C. H., and Yin, S. L., "A Novel Hyperbolic Grid Generation Procedure with Inherent Adaptive Dissipation," *Journal of Computational Physics*, Vol. 116, No. 1, 1995, pp. 173–179.

[16]Tai, C. H., Chiang, D. C., and Su, Y. P., "Three-Dimensional Grid Generation with Inherent Dissipation and Laplacian Smoothing," *AIAA Journal*, Vol. 34, No. 9, 1996, pp. 1801–1806.

[17]Winslow, A. M., "Numerical Solution of the Quasi Linear Poisson Equation in a Nonuniform Triangle Mesh," *Journal of Computational Physics*, Vol. 2, No. 2, 1967, pp. 149–172.

[18]Brackbill, J. U., and Saltzman, J. S., "Adaptive Zoning for Singular Problems in Two Dimensions," *Journal of Computational Physics*, Vol. 46, No. 3, 1982, pp. 342–368.